EXPERIMENTAL LOW-SPEED AERODYNAMIC

CHARACTERISTICS OF THE WORTMANN

FX 66-S-196 V1 AIRFOIL

by

J. H. M. Gooden
Department of Aerospace Engineering,
Delft University of Technology, The Netherlands

SUMMARY

An investigation to obtain the two-dimensional aerodynamic characteristics of the FS 66-S-196 V1 airfoil was performed. Pressure distributions have been measured at Reynolds numbers ranging from 0.5×10^6 to 2.0×10^6 at angles of attack between -6 and +20 degrees. An oil film technique and stethoscope investigations were used to determine respectively the position of the laminar separation bubble and transition.

The measurements were supported by potential-flow calculations (with and without walls) using a two-dimensional panel method. Comparison of the calculated results in both cases shows that the tunnel wall interference is small at the given tunnel width-over-chord ratio of 4.6. The measured results have been compared with those given in the Stuttgarter Profilkatalog (Ref. 2).

Some conclusions indicated by the investigations are:

. The maximum lift coefficient decreases from 1.57 to 1.48 at Reynolds numbers between 0.5×10^6 and 2.0×10^6.

. The lift coefficient decreases sharply as the angle of attack exceeds the value for maximum lift. The stall is of the trailing edge type.

. The drag coefficient is about 0.5×10^{-3} smaller than the value given in Ref. 2. Also the low drag range extends to slightly higher values of the lift coefficient.

. The airfoil drag is very sensitive to small dust particles collecting on the surface of the airfoil in the nose region: an increase in drag of 20 to 50% has been measured at higher values of the angle of attack ($\alpha > 5°$).

. The value of the pitching-moment coefficient about the quarter-chord point is nearly constant and equals -0.11 as long as no trailing edge separation occurs.

SYMBOLS

A	geometric aspect ratio of two-dimensional model in tunnel (Fig. 1); s/c
b	effective tunnel width, m; S/h
C_p	pressure coefficient; $\dfrac{p-p_m}{q_m}$

c — airfoil chord, m

c_d — section profile drag coefficient, determined from wake measurements

c_ℓ — section lift coefficient; calculated from

$$\frac{c_n}{\cos \alpha} - c_d \cdot \tan \alpha$$

c_{ℓ_α} — section lift-curve slope

$c_{\ell_{\alpha_o}}$ — section lift-curve slope at $\alpha = 0°$

$c_{m_{0.25c}}$ — section pitching-moment coefficient about quarter chord point, positive in nose up direction; calculated from

$$-\oint_C c_p \left(\frac{x}{c} - 0.25 \right) d\left(\frac{x}{c} \right)$$

c_n — section normal-force coefficient; calculated from

$$\oint c_p \, d\left(\frac{x}{c} \right)$$

D — section drag force, N

h — height of test section, m

L — section lift force, N

p — local static pressure, N/m^2

p_m — "effective" static pressure, defined as mean value of tunnel wall static pressures, N/m^2

p_t — undisturbed total pressure, N/m^2

q_m — "effective" dynamic pressure, N/m^2; $p_t - p_m$

R_c — Reynolds number based on "effective" free stream conditions and airfoil chord; $\sqrt{\dfrac{2q_m}{\rho}} \dfrac{c}{\nu}$

S — cross-sectional area of test section, m^2

s — model span, m

X — airfoil abscissa, m

Y — airfoil, m

α — angle of attack, angle between longest chord and free stream direction, deg.

α_o — angle of attack at zero lift, deg.

Δc_ℓ — increment in lift coefficient due to presence of tunnel walls

ν — coefficient of kinematic viscosity, m^2/s

ρ — air density, kg/m^3

Subscripts

max — maximum

w — conditions in presence of walls

∞ — free stream conditions

Abbreviations

C — airfoil contour

1 — lower surface

L.E. — leading edge

R — reattachment

S — separation

T — transition

T.E. — trailing edge

u — upper surface

Chord definition:
    Chord line is the longest line connecting the forward and rearward extremeties of the airfoil contour, i.e. longest chord.

INTRODUCTION

The FX 66-S-196 V1 airfoil was designed by Prof. F. X. Wortmann of the University of Stuttgart. It is one specimen of a wide selection of airfoils, presented in Ref. 2, in most cases designed especially for application in sailplanes. Most of these airfoils are characterized by a wide low drag range and -- at the same time -- a high maximum lift coefficient corresponding to the requirements

of sailplane design.

The present airfoil was chosen for investigations to provide more data for sailplane performance calculations (Ref. 10). Another reason was the possibility to gain further knowledge on laminar separation bubbles in order to refine a viscous-flow airfoil computer program. Therefore, the airfoil model had a high accuracy and was equipped with a large number of pressure taps in order to allow accurate measurements of the pressure distributions.

Tests included flow investigations and determination of the basic, two-dimensional, low-speed characteristics at Reynolds numbers ranging from 0.5×10^6 to 2.0×10^6. Special care was devoted to a correct measurement of the angle of attack. Therefore also measurements were carried out with the model inverted (Ref. 7). The model was tested in smooth condition only.

MODEL, APPARATUS AND TEST PROCEDURES

Model Description

The wind tunnel model was manufactured by means of a method recently developed at the Department of Aerospace Engineering (Ref. 3). According to this method the model was casted in three equal, spanwise parts using a movable, accurate mould. Casting material used was the synthetic resin "Araldit". Preliminary investigations indicated that the burrs between the three parts did have only minor or no influence to the airflow.

The model has a chord length of 0.360 m and is positioned vertically, spanning the tunnel height which equals 1.25 m (Fig. 1). The design airfoil coordinates are given in Table 1. The design coordinate at 99.893%
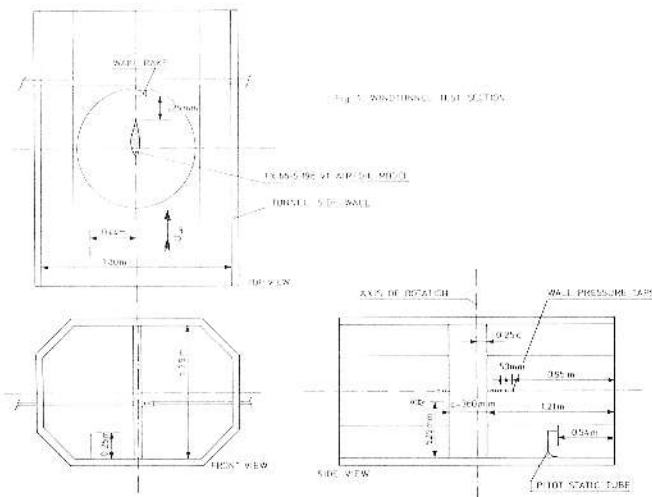

TABLE 1. Airfoil Coordinates FX 66-S-196 V1 (Design)

x/c (%)	y/c (%)	x/c (%)	y/c (%)
100.000	0.0	0.0	0.0
99.893	0.039	0.107	-0.354
99.039	0.284	0.428	-0.784
97.347	0.729	0.961	-1.211
94.844	1.357	1.704	-1.639
91.573	2.193	2.653	-2.065
87.592	3.242	3.806	-2.489
85.355	3.845	5.156	-2.903
82.967	4.501	6.699	-3.307
80.438	5.197	8.427	-3.695
77.779	5.936	10.332	-4.063
75.000	6.699	12.408	-4.410
72.114	7.482	14.645	-4.729
69.134	8.272	17.033	-5.022
66.072	9.067	19.562	-5.279
62.941	9.844	22.221	-5.503
59.755	10.607	25.000	-5.681
56.526	11.321	27.866	-5.820
53.270	11.995	30.866	-5.901
50.000	12.585	33.928	-5.931
46.730	13.095	37.059	-5.880
43.474	13.467	40.245	-5.743
40.245	13.691	43.474	-5.451
37.059	13.690	46.730	-5.076
33.928	13.537	50.000	-4.628
30.866	13.243	53.270	-4.161
27.866	12.848	56.526	-3.667
25.000	12.348	59.755	-3.186
22.221	11.772	62.941	-2.707
19.562	11.114	66.072	-2.256
17.033	10.398	69.134	-1.827
14.645	9.621	72.114	-1.435
12.408	8.803	75.000	-1.080
10.332	7.946	77.779	-0.764
8.427	7.067	80.438	-0.489
6.699	6.170	82.967	-0.260
5.156	5.273	85.355	-0.068
3.806	4.383	87.592	0.080
2.653	3.520	91.573	0.254
1.704	2.691	94.844	0.288
0.961	1.918	97.347	0.206
0.428	1.223	99.039	0.066
0.107	0.621	100.000	0.0

chord, lower surface, as given in Ref. 2, has been left out because of the fact that this point fitted poor to the adjacent ones. Figure 2 shows the design airfoil shape; the x-axis coincides with the airfold chord.

Preliminary investigations showed that model-tolerances are within 0.1 mm. The model is equipped with 107 pressure orifices drilled perpendicular to the local model surface. All pressure orifices have a diameter of 0.4 mm nominal.
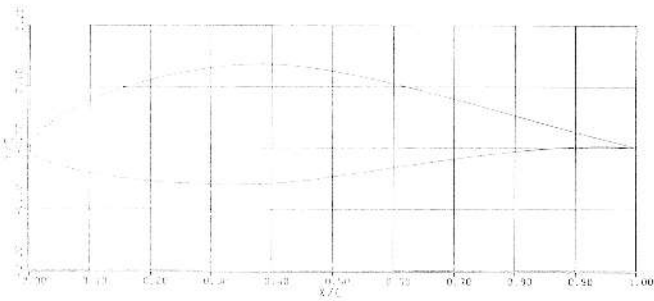
Fig.2 FX33-5 190 V1 (HEIGHT CONTOUR

Wind Tunnel and Model Support

The low-speed low-turbulence wind tunnel of the Department of Aerospace Engineering at Delft University of Technology is of the closed return type and has an octagonal test-section (Fig. 1) of the 1.80 m wide and 1.25 m high. The cross-sectional area of the test section equals 2.07 m^2, yielding a mean tunnel width of 1.656 m. The test section has solid walls and is equipped with two turntables, 1.15 m in diameter. These turntables are flush with the tunnel walls and provide attachment of the model by means of rectangular model end-plates. The center of rotation of the model is located at a position of 3 percent chord above the quarter-chord point.

The turbulence level in the test section varies between 0.025% at 40 m/s and 0.085% at 100 m/s. A further detailed description of the tunnel is given in Ref. 4.

Instrumentation

Wall pressures were measured at 15 stations, located in the plane of the mid-chord section, on each tunnel sidewall. The position of these stations, equally spaced at 50 mm, was symmetrical with respect to the quarter-chord point of the model (Fig. 1).

The pitot-static tube was placed 0.75 m in front of the model rotation axis and 0.44 m out of the vertical plane of symmetry in the model upper surface direction. Its height was 0.25 m and it was placed on the floor of the test section.

A wake survey rake, mounted on a cross beam, was positioned perpendicular to the vertical plane of symmetry and 0.10 m below the mid-span section containing the pressure taps. The tips of the total pressure tubes were at 0.63 chord length downstream of the model trailing edge (at $\alpha = 0°$). The wake rake employed 17 total-pressure tubes, 1.5 mm in diameter, and 4 static-pressure tubes, 3.2 mm

in diameter. The total-pressure tubes were equally spaced at 2.5 mm.

All pressures, including the static pressure on the model surface were obtained using an automatic reading multitube liquid manometer (200 tubes).

Tests and Data Reduction Procedures

The airfoil was tested at Reynolds numbers from 0.5 x 10^6 to 2.0 x 10^6. The angle of attack was varied between -6 and +20 degrees. Pressure distributions were measured and the nature of the airfolow on the model surface was examined by means of an oil-film technique. Stethoscope investigations were carried out to determine the position of transition. The model was tested with smooth surfaces only.

The static pressure measurements on the airfoil surface were reduced to standard pressure coefficients and then integrated to get section normal force and pitching-moment coefficient. Section profile-drag coefficients were obtained from the wake-rake pressures using the method of Squire-Young as described by Pfenninger (Ref. 5). The lift coefficient was determined using the relation:

$$c_\ell = \frac{c_n}{\cos \alpha} - c_d \cdot \tan \alpha$$

The spanwise drag distribution at cross-sections within a distance of 0.15 m to the mid-chord section was investigated at $R_c = 1.5$ x 10^6 and $\alpha = 0°$. It appeared that the spanwise drag distribution was not entirely uniform. Behind the pressure orifice section a 9% higher drag was measured while just beside this section the drag was about 15% smaller compared to the undisturbed drag. Stethoscope investigations showed less than 1 to 2 percent chord difference in the position of transition between the mid-chord section and other sections. This non-uniformity in the drag distribution was found to extend over a region of about 0.10 m wide in the spanwise direction (at the given distance of the tips of the wake-rake total-pressure tubes behind the trailing edge). In order to assure a reliable measurement of the airfoil drag the wake-rake was placed 0.10 m below the plane of the mid-span section.

Tunnel Wall Interference

In order to estimate the influence of the tunnel walls on the pressure distributions and the lift coefficient a computer program was developed using a two-dimensional panel method (Ref. 6). Some results of these incompressible, inviscid calculations are

presented in Fig. 3 and 4. They are valid for the actual tunnel-width over airfoil-width over airfoil-chord ratio of 4.6 only.

Fig. 3 shows the change in c_ℓ, at a given angle of attack, due to the presence of the tunnel walls. The value of $\Delta c_\ell / c_\ell$ amounts to about 2%. c_ℓ and c_{ℓ_w} were determined from pressure distributions with reference pressure: p_∞. The influence of the tunnel walls on the potential flow pressure distribution, at an angle of attack of 6 degrees, is shown in Fig. 4. In this figure two pressure distributions are shown, with and without walls, using p_∞ as reference pressure.
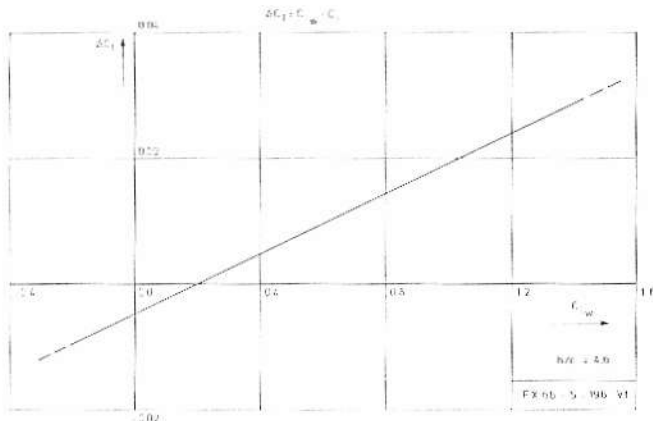
Fig 3 EFFECT OF WINDTUNNEL WALL INTERFERENCE ON POTENTIAL FLOW LIFT COEFFICIENT AT A GIVEN ANGLE OF ATTACK
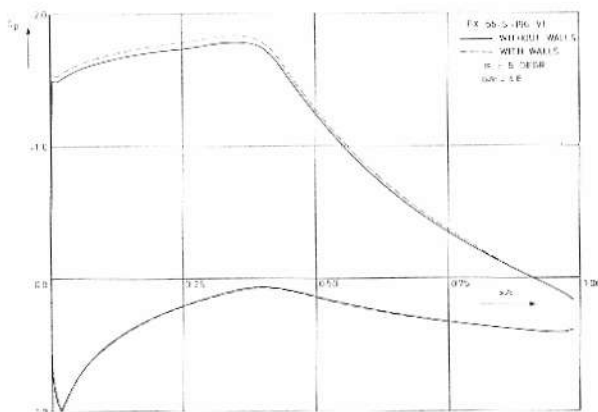
Fig 4 EFFECT OF WINDTUNNEL WALL INTERFERENCE ON POTENTIAL FLOW DISTRIBUTION

Differences between the two pressure distributions are small but increase with increasing angle of attack. During the data reduction a blockage correction has been taken into account by using p_m, the "effective" static pressure, as reference pressure. p_m was determined as the mean of all wall-pressures

measured. Using the calculated p_m as reference pressure a potential flow pressure distribution is found, situated just below the one without walls. No further standard low-speed wind tunnel corrections are applied because they are within the accuracy of the measurements. Angle of attack correction, related to model alignment, has been achieved by means of measurements with the model inverted (Ref. 7).

Additional Calculations

On the airfoil nose an inviscid flow pressure distribution has been matched to the measured pressure distribution in order to catch any pressure peaks which might develop there. Analogous to the procedure presented in Ref. 8, the potential flow was fitted to the actual flow by means of disregarding the Kutta-condition. The circulation was adjusted such that the potential flow pressure corresponded to the measured pressure at a reference pressure orifice on the airfoil nose. This method seems justified because the boundary layer thickness -- and therefore the displacement thickness -- is very small on the airfoil nose thus causing only slight differences between the actual and fitted potential flow pressure distributions.

In the trailing edge region a parabolic extrapolation of the pressure distribution was performed, based on the three most backward situated measured pressures. The mean value of these extrapolations on upper and lower surface at the trailing edge was used in calculating the basic airfoil coefficients.

PRESENTATION OF RESULTS

Pressure Distributions

A large number of measured pressure distributions is given in Ref. 9. Some examples are shown here, in which the presence of a laminar separation bubble is clearly marked, especially on the upper surface. This laminar separation bubble usually occurs just behind the pressure minimum. The pressure distribution at the location of the bubble shows an almost flat part between separation and transition and a subsequent steep pressure recovery between transition and reattachment (Fig. 5). Transition and reattachment are clearly marked because of a rather abrupt change in chord-wise pressure gradient. They can therefore, easily be determined from the pressure distribution if the model is equipped with a sufficient number of pressure orifices.
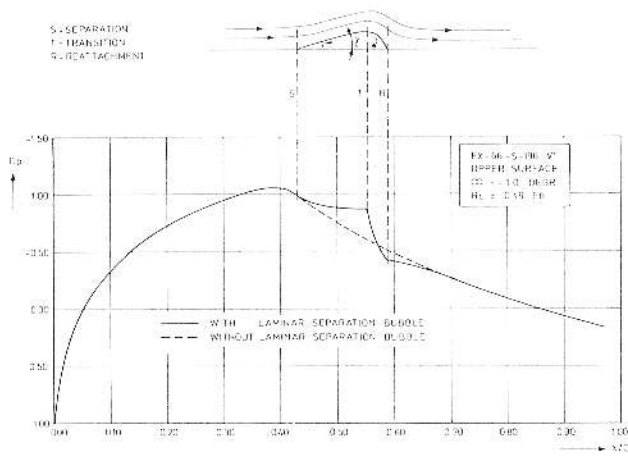
Remarkable is the extreme flat pressure

Fig. 5 EFFECT OF LAMINAR SEPARATION BUBBLE ON PRESSURE DISTRIBUTION

distribution between 5 and 40 percent chord occurring at $\alpha = -2°$ (Fig. 6.2) on the lower surface. Such a pressure distribution occurs also on the upper surface at $\alpha = 8°$ (Fig. 6.3),

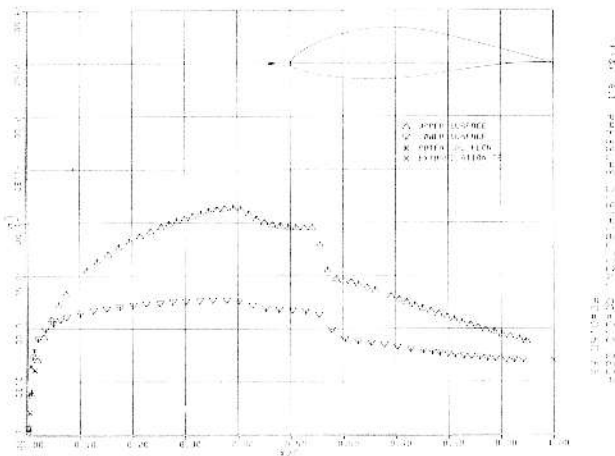except for a small pressure peak developing on the airfoil nose. This pressure peak, however, does not lead to separation or transition of the laminar boundary layer because, at all Reynolds numbers investigated, laminar separation occurs at 41% chord leading to a laminar separation bubble. Possibly, $\alpha = -2°$ and $+8°$, being about the boundaries of the low drag range, were the design angles of attack for the lower and upper surfaces, respectively (Ref. 1).

Flow Behavior

The behavior of the airflow on the model surface was investigated by means of an oil-film technique and a stethoscope at Reynolds numbers of 0.5×10^6 and 1.5×10^6. The results are in good agreement when comparing pressure distributions with oil-flow patterns. Determination of transition by means of a stethoscope usually gave results about 1 or 2 percent chord aft of the transition location indicated by the pressure distribution.

Fig. 7 shows the oil-flow pattern, at $\alpha = 0°$ and a Reynolds number of 0.5×10^6, on the model lower surface. The corresponding pressure distribution is given in Fig. 6.1. The position of laminar separation, transition and reattachment is marked in the picture. It should be remarked that the model is positioned vertically, causing the oil substance to display vertical tracks if the wall shear stress is zero, for instance at laminar separation.

The position of laminar separation, transition and reattachment, for Reynolds numbers of 0.5×10^6 and 1.5×10^6, are given in Fig. 8. It seems that, in both cases, the laminar separation bubble is situated on the airfoil nose, lower surface at $\alpha = -6°$. If the angle of attack is increased it at first disappears and then appears again if the angle
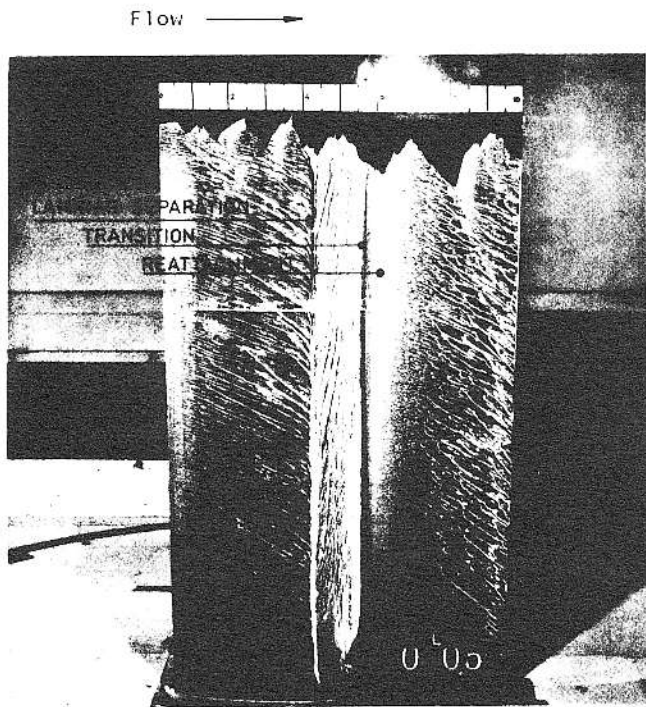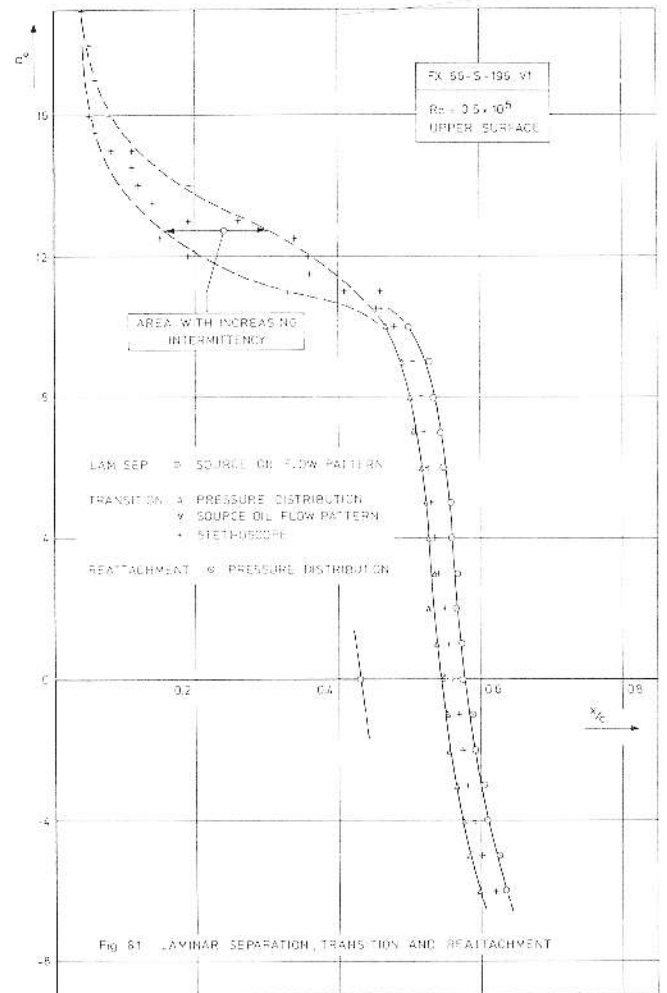
Flow ⟶

angle of attack = 0°   Rc = 0.5*10⁶

lower surface

Fig.7 Oil-flow pattern

Fig. 81   LAMINAR SEPARATION, TRANSITION AND REATTACHMENT

of attack is further increased. On the upper surface the bubble is present until the angle of attack is increased to the value for maximum lift. The bubble length as well on the upper as on the lower surface amounts to about 15 percent chord at R_c = 0.5 x 10⁶ and to about 7 percent chord at R_c = 1.5 x 10⁶.

Initially at an angle of attack between 6 and 7 degrees a pressure peak develops on the airfoil nose. This pressure peak increases with increasing angle of attack and causes transition to move forward at angles of attack just below the value for maximum lift. This, in turn, causes a thickening of the turbulent boundary layer at the trailing edge, which ultimately leads to turbulent separation. Turbulent separation then moves rapidly forward to 45% chord at an angle of attack of 15 degrees. Between α = 10° and α = 15° no stationary pressure distribution is present.

Transition sweeps up and down on a chord traject of about 15 percent, thus causing on area with increasing intermittency. At angles of attack above 15 degrees the flow becomes more stationary again.

Section Lift, Drag and Pitching
Moment Characteristics

Section lift curves are given in Fig. 9. The value of the lift-curve slope, $C_{l_{\alpha_0}}$, increases from 0.112 per degree at R_c = 0.5 x 10⁶ to 0.118 at R_c = 2.0 x 10⁶ due to decreasing viscous influences at higher Reynolds numbers. These values are clearly higher than those given in Ref. 2 (Fig. 14). This probably is due to the smaller geometric model aspect ratio, used in Ref. 2 (A ≈ 1.5), leading to an increased influence of the vortices trailing off near the tunnel walls on the flow about the mid-chord section.

The value of α_0 nearly remains constant with Reynolds number. Its mean value is -4.3°.
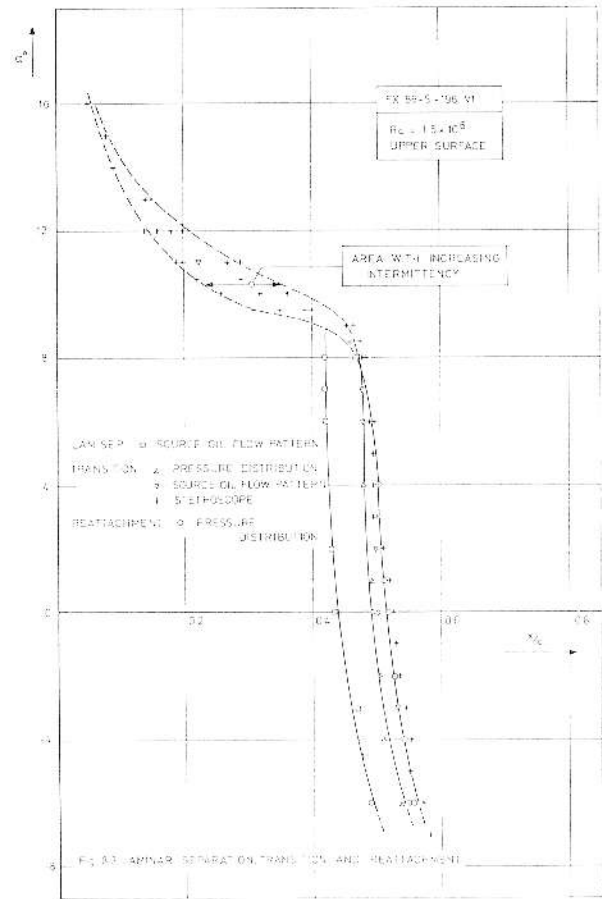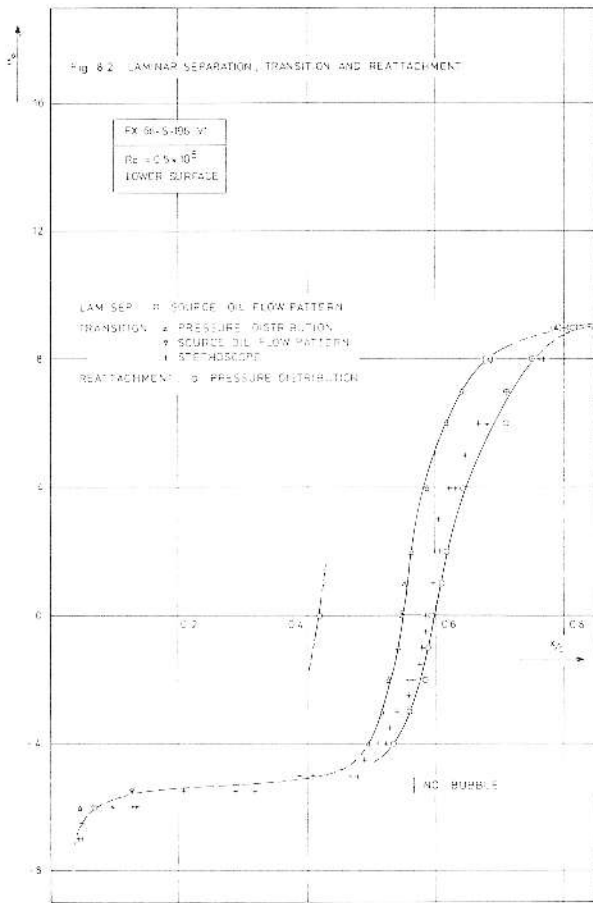
This value is 0.3° higher than the value given in Ref. 2, probably due to differences in airfoil contour or chord definition.

The value of $c_{\ell_{max}}$ decreases with increasing Reynolds number because of a forward movement of transition with increasing Reynolds number. This, in turn, has a thickening effect on the turbulent boundary layer thus causing it to separate earlier. The values of $c_{\ell_{max}}$ correspond well to those given in Ref. 2, except for the one at $R_c = 1.0 \times 10^6$ (Fig. 14).

Fig. 10 shows the section drag characteristics. Roughly speaking, the lift drag curves consist of two straight parts, connected at $c_{\ell} \approx 0.5$, with regions of higher or lower drag appearing at the ends of the low-drag range. Flow investigations did not reveal any clarification for this behavior. From the location of transition and the position of the center of the wake it is suggested, however, that this phenomena is caused by a shifted alteration of the upper and lower surface drag. Further experimental investigations are needed to support this argument.

Comparison of the drag characteristics with those given in Ref. 2 shows that the present values of the drag coefficient are, in general, about 0.5×10^{-3} smaller than those given in Ref. 2. Also the low drag range extends to somewhat higher values of c_{ℓ}. These differences might be originating from differences in tolerances between the models used.

The maximum value of L/D depends on the Reynolds number and varies between 105 and 158 (Fig. 11). These values appear at angles of attack just below that for maximum lift. Fig. 12 gives the maximum value of the sinking speed parameter c_{ℓ}^3/c_d^2 at different Reynolds numbers.

Pitching moment characteristics (Fig. 13) show a nearly constant pitching-moment coefficient about the quarter-chord point as long as no turbulent separation occurs. This

Fig 8A: LAMINAR SEPARATION, TRANSITION AND REATTACHMENT

Fig. 9. FX 66-S-196 V1 SECTION LIFT CHARACTERISTICS
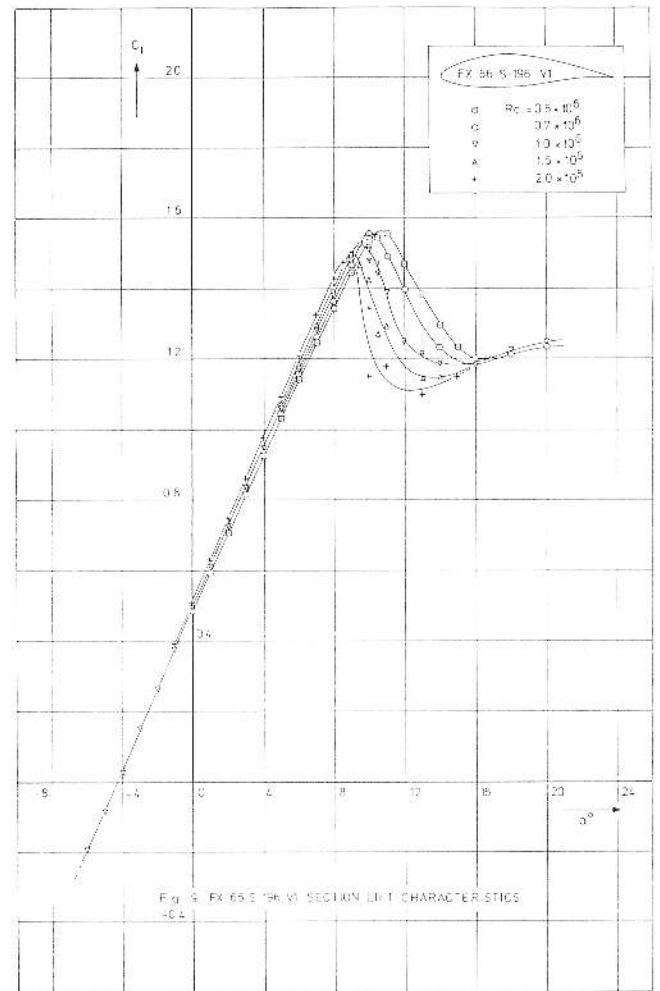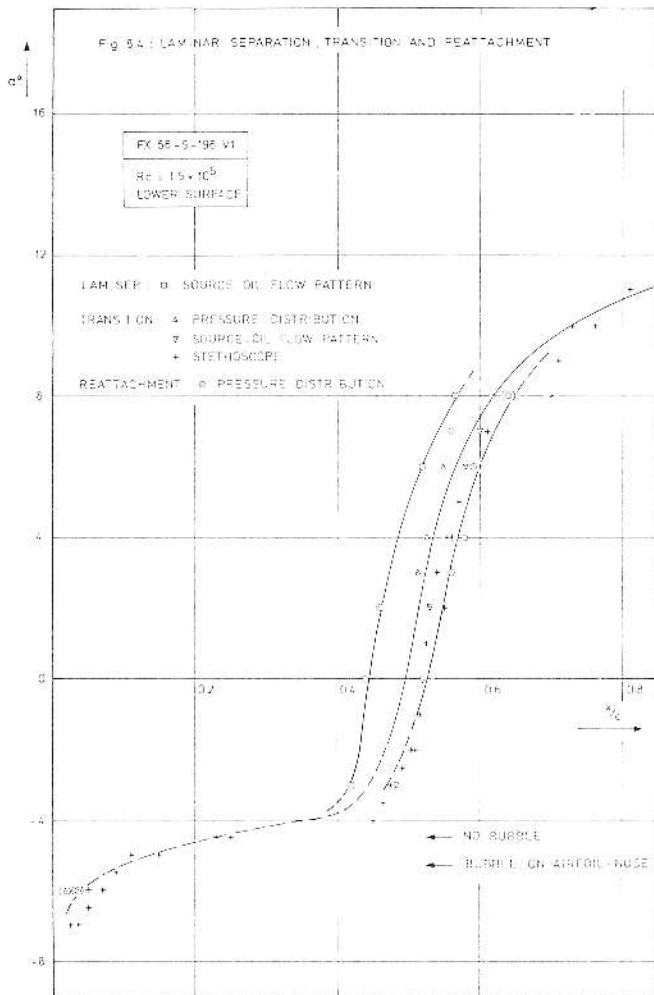
indicates that the aerodynamic center lies close to the quarter-chord point. Only slight variations occur when the Reynolds number is changed.

Sensitivity to Surface Contamination

Finally, it is remarked that the airfoil under investigation is very sensitive to contamination of the airfoil leading edge. Small roughness particles cause a turbulent wedge that destroys the laminar flow and thickens the turbulent boundary layer. This ultimately may lead to the onset of turbulent separation and corresponding loss of lift. An increase of 20 to 50 percent in c_d has been measured at higher values of the lift coefficient ($c_\ell > 1.1$ at $R_c = 1.5 \times 10^6$). This increase in drag was caused by a small oxide particle, stuck to the model upper surface in the plane of the wake rake and downstream of the airfoil nose at about 3 percent chord. Because of this effect, special care

was taken that the model was clean during the measurements.

CONCLUSIONS

An investigation has been conducted in the low-speed, low-turbulence wind tunnel at the Department of Aerospace Engineering of Delft University of Technology in order to determine the basic, two-dimensional aerodynamic characteristics on an accurate model of the FX 66-S-196 V1 airfoil. The resulting data have been compared with those given in the "Stuttgarter Profilkatalog" (Ref. 2). The airfoil was tested with smooth surface only in an angle of attack range from -6 to +20 degrees and Reynolds numbers between 0.5×10^6 and 2.0×10^6.

Some conclusions indicated by the investigation are:

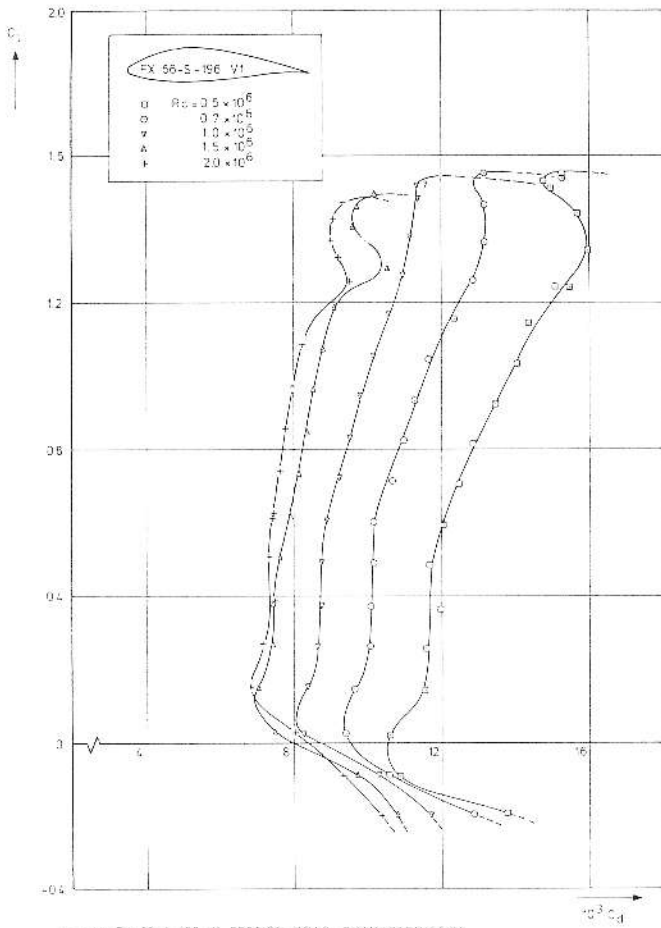. The maximum value of the lift coefficient

Fig. 10 FX 66-S-196 V1 SECTION DRAG CHARACTERISTICS
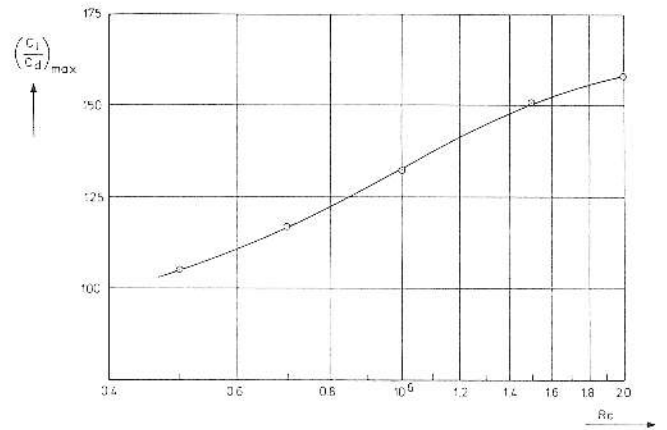

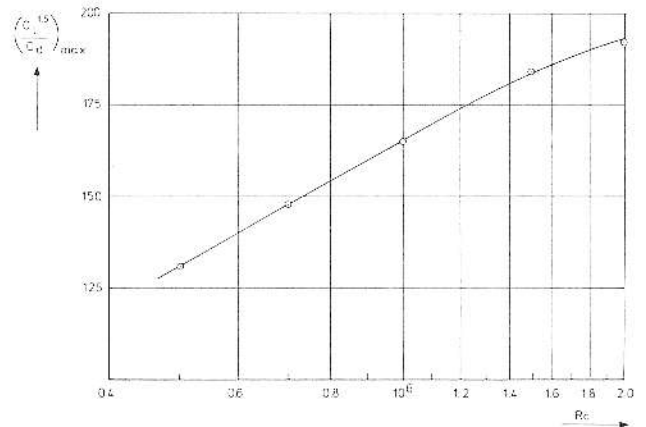Fig. 11 VARIATION OF MAX. LIFT TO DRAG RATIO WITH REYNOLDS-NUMBER

Fig. 12 VARIATION OF THE MAX. VALUE OF THE SINKING SPEED PARAMETER WITH REYNOLDS-NUMBER

decreases from 1.57 to 1.48 at Reynolds numbers between 0.5×10^6 and 2.0×10^6.

. The lift coefficient decreases sharply as the angle of attack exceeds the value for maximum lift while turbulent separation moves forward fast to 40 to 45% chord, starting from the trailing edge.

. The value of the lift-curve slope is clearly larger than the value given in Ref. 2, probably because of the difference in geometric model aspect ratio.

. The drag coefficient is about 0.5×10^{-3} smaller compared to that given in Ref. 2. Also the low-drag range extends to slightly higher values of c_ℓ.

. It appeared that the airfoil is very sensitive to small dust particles collecting on the surface in the nose
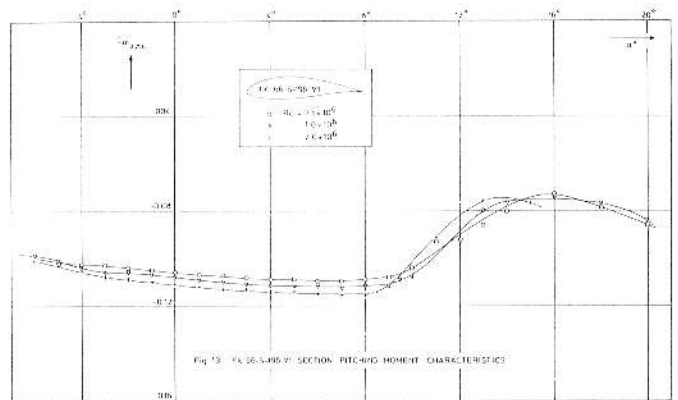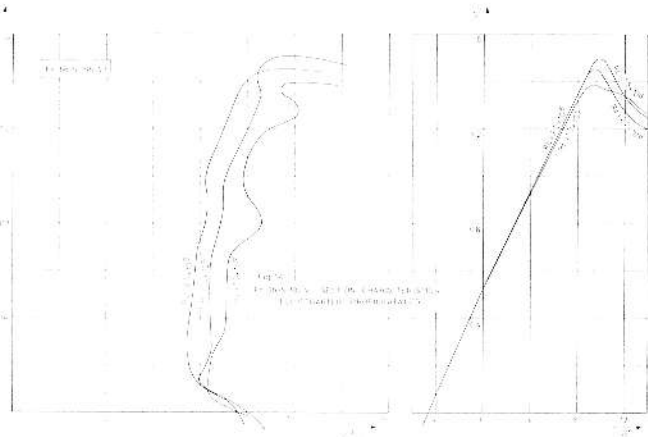

Fig. 13 FX 66-S-196 V1 SECTION PITCHING MOMENT CHARACTERISTICS

region. An increase in drag of 20 to 50% has been measured at higher lift coefficients at $R_c = 1.5 \times 10^6$.

. A laminar separation bubble usually occurs at 40 to 50% chord. In some

30

cases it lies on the airfoil nose
(e.g. $\alpha = -6°$, $R_c = 0.5 \times 10^6$, lower
surface), in other cases it is absent
(e.g. $\alpha = 4.5°$, $R_c = 1.5 \times 10^6$, lower
surface).

. The value of the pitching-moment co-
efficient about the quarter-chord point
is about -0.11 at all Reynolds numbers
investigated, as long as no turbulent
separation occurs.

ACKNOWLEDGEMENT

REFERENCES

1. Wortmann, F. X., A critical review of the
physical aspects of airfoil design at low
Mach numbers, NASA CR-2315, pp. 179-196,
1972.

2. Althaus, D., Stuttgarter Profilkatalog I,
Institut für Aero-und Gasdyamik der
Universität Stuttgart, 1972.

3. Heuven, M. H. W. van, A relatively cheap
method of producing two-dimensional wind
tunnel models of synthetic material with
poured-in pressure lines, Report VTH-202,
Department of Aerospace Engineering,
Delft University of Technology, 1975
(in Dutch).

4. Dobbinga, E., and Ghesel Grothe, J. A. van,
The low speed wind tunnel of the Depart-
ment of Aerospace Engineering at Delft
University of Technology, De Ingenieur,
1955 (in Dutch).

5. Pfenninger, W., Vergleich der Impulsmethode
mit der Wägung bei Profilwiderstandsmes-
sungen, Mitteilung 8 der ETH, Zürich, 1973.

6. Gooden, J. H. M., A numerical method of
calculating two-dimensional wind tunnel
wall interference on multi-element air-
foils in incompressible, inviscid flow,
Report to be published, Department of
Aerospace Engineering, Delft University
of Technology, 1978.

7. Pope, A., and Harper, J. J., Low speed
wind tunnel testing, John Wiley & Sons
Inc., New York, 1966.

8. Boermans, L. M. M., and Blom, J. J. H.,
Low-speed aerodynamic characteristics
of an 18% thick airfoil section designed
for the all-flying tailplane of the M-300
sailplane, Report LR-226, Department of
Aerospace Engineering, Delft University
of Technology, 1976.

9. Gooden, J. H. M., Experimental low-speed
aerodynamic characteristics of the
Wortmann FX 66-S-196 V1 airfoil, Report
to be published, Department of Aerospace
Engineering, Delft University of Tech-
nology, 1978.

10. Boermans, L. M. M., Development of a
computer program for parametric sailplane
performance optimization, OSTIV Congress,
Châteauroux, 1978.